Ex-situ Measurement of Internal Deformation in Ball Grid Array Package with Digital Volume Correlation

WANG Long[1], *GAO Zizhan*[2*], *ZHANG Xuanhao*[2], *LIU Qiaoyu*[1], *HOU Chuantao*[1], *XING Ruisi*[1]

1. Science and Technology on Reliability and Environmental Engineering Laboratory, Beijing Institute of Structure and Environment Engineering, Beijing 100076, P. R. China;
2. National Key Laboratory of Strength and Structural Integrity, School of Aeronautic Science and Engineering, Beihang University, Beijing 100191, P. R. China

(Received 21 August 2024; revised 10 October 2024; accepted 15 October 2024)

Abstract: In spacecraft electronic devices, the deformation of solder balls within ball grid array (BGA) packages poses a significant risk of system failure. Therefore, accurately measuring the mechanical behavior of solder balls is crucial for ensuring the safety and reliability of spacecraft. Although finite element simulations have been extensively used to study solder ball deformation, there is a significant lack of experimental validation, particularly under thermal cycling conditions. This is due to the challenges in accurately measuring the internal deformations of solder balls and eliminating the rigid body displacement introduced during ex-situ thermal cycling tests. In this work, an ex-situ three-dimensional deformation measurement method using X-ray computed tomography (CT) and digital volume correlation (DVC) is proposed to overcome these obstacles. By incorporating the layer-wise reliability-guided displacement tracking (LW-RGDT) DVC with a singular value decomposition (SVD) method, this method enables accurate assessment of solder ball mechanical behavior in BGA packages without the influence of rigid body displacement. Experimental results reveal that BGA structures exhibit progressive convex deformation with increased thermal cycling, particularly in peripheral solder balls. This method provides a reliable and effective tool for assessing internal deformations in electronic packages under ex-situ conditions, which is crucial for their design optimization and lifespan predictions.

Key words: ball grid array (BGA) packages; digital volume correlation; ex-situ; rigid body displacement; thermal cycling test

CLC number: O348.1 **Document code:** A **Article ID:** 1005-1120(2024)05-0609-12

0 Introduction

Spacecrafts, such as launch vehicles, are equipped with a large number of electronic products that exhibit significant differences in structural morphology due to their different functions[1]. Despite these differences, these electronics often contain a common core element — The central computing unit chip that handles data processing. To ensure the safe operation of these chips and their connections to the carrier, they are typically housed in an integrated electronic package structure. The stable operation of this packaging structure in complex service environments, especially in thermal cycling environment, is crucial for maintaining the safety and reliability of spacecraft[2-4].

As electronic product design increasingly trends towards miniaturization and high preference, electronic packaging technologies have been subject to continuous innovation, adapting to different technological requirements. Among various packaging technologies, ball grid array (BGA)

*Corresponding author, E-mail address: gaozizhan@buaa.edu.cn.

How to cite this article: WANG Long, GAO Zizhan, ZHANG Xuanhao, et al. Ex-situ measurement of internal deformation in ball grid array package with digital volume correlation[J]. Transactions of Nanjing University of Aeronautics and Astronautics, 2024, 41(5): 609-620.

http://dx.doi.org/10.16356/j.1005-1120.2024.05.006

packages are used in microelectronic manufacturing industries, using solder balls instead of traditional leads at the bottom of the electronic package[5]. These solder balls play a key role in signal transmission between the chip and the main body of the BGA package. However, the long-term thermal cycling under service environment may lead to deformation of solder balls, damping the stability of signal transmission. Therefore, it is critical to characterize the mechanical behavior of solder balls under thermal cycling loading to ensure the safe and reliable use of BGA backage. This characterization will also facilitate design optimization, improve manufacturing processes, and enhance the accuracy of strength and lifespan predictions for BGA packages[6-7].

Nevertheless, most studies on the mechanical properties of solder balls under thermal cycling are predominantly based on finite element simulations, with limited real experimental validation[8-9]. This reliance stems from the limitations of commonly used deformation measurement techniques, such as digital image correlation (DIC), which are only capable of capturing surface deformation[10]. In the case of solder balls, their deformation is obscured by surrounding support materials, such as plastic and ceramic, making direct observation and measurement difficult. Consequently, these methods cannot capture internal deformations without compromising the structural integrity of the package. There remains a shortage of real experimental research on the mechanical behavior of solder balls under thermal cycling conditions.

To capture the three-dimensional internal deformation of bone under mechanical loading, the digital volume correlation (DVC) method was developed[11]. This method involves matching three-dimensional volumetric images obtained via X-ray computed tomography (CT) before and after deformation, enabling the extraction of deformation data for internal calculation points within the volume. Over the past several decades, the DVC method has been successfully applied across various disciplines[12-18]. Therefore, DVC is expected to be an effective means for measuring the deformation of BGA solder balls.

Typically, the DVC method is used to characterize the internal deformation field and its evolution process inside the material under in-situ loading conditions. The measured deformation representing the true deformation of the specimen[12,14,19]. However, the limited specimen accommodation space in the CT scanning equipment and the long total test time required by the thermal cycling loading process make it difficult to synchronize the thermal cycling loading with the in-situ CT scanning in the same spatiotemporal framework. Consequently, for standard thermal cycling tests, the package structure can only undergo offline ex-situ X-ray CT scanning after experiencing varying numbers of thermal cycles. Ex-situ scanning introduces unknown rigid body displacement, preventing the DVC method from accurately extracting the true deformation of solder balls. To estimate the rigid body displacement introduced by ex-situ scanning, the outer image registration method has been proposed[20]. Nevertheless, due to the small size of the scanned BGA package, the large reference block used in this method reduces the scanning resolution and may detach under significant temperature differences during loading. In view of this, there is a need for a new method without reference sample to measure the true deformation of BGA balls under thermal cycling loading conditions.

To address this issue, the ex-situ 3D image measurement method for the internal deformation in BGA package based on X-ray CT and DVC method has been proposed in this paper. A layer-wise reliability-guided displacement tracking (LW-RGDT) strategy based DVC method[21] is combined with a singular value decomposition (SVD) based rigid body displacement elimination method to propose an ex-situ deformation measurement method for BGA package. The effectiveness of this method in eliminating rigid body displacement is verified through simulated rigid body displacement experiments. The deformation results indicate that, following thermal cycling, the BGA structure exhibits a convex deformation that increases with the number of cycles. Solder balls at the periphery of the BGA package undergo greater deformation, which aligns with the temperature variations from low to

ambient temperatures observed at the conclusion of the thermal cycling process.

1 Experimental Method

1.1 BGA package sample

The chip model selected in this work is Samsung-KLM8G1GETF-B041[22], with a BGA package type. The package size is 11.5 mm×13 mm×0.8 mm, the diameter of a single solder ball is about 0.3 mm, and 153 solder balls are included as shown in Fig.1. The letters and numbers in the image represent the labels for the rows and columns of the solder balls. The circuit board and chip were prepared using standard surface mount technology (SMT) processes. The PCB material is FR-4 epoxy resin/glass fiber, the pad material is copper, and the solder balls are 63/37 tin-lead solders.

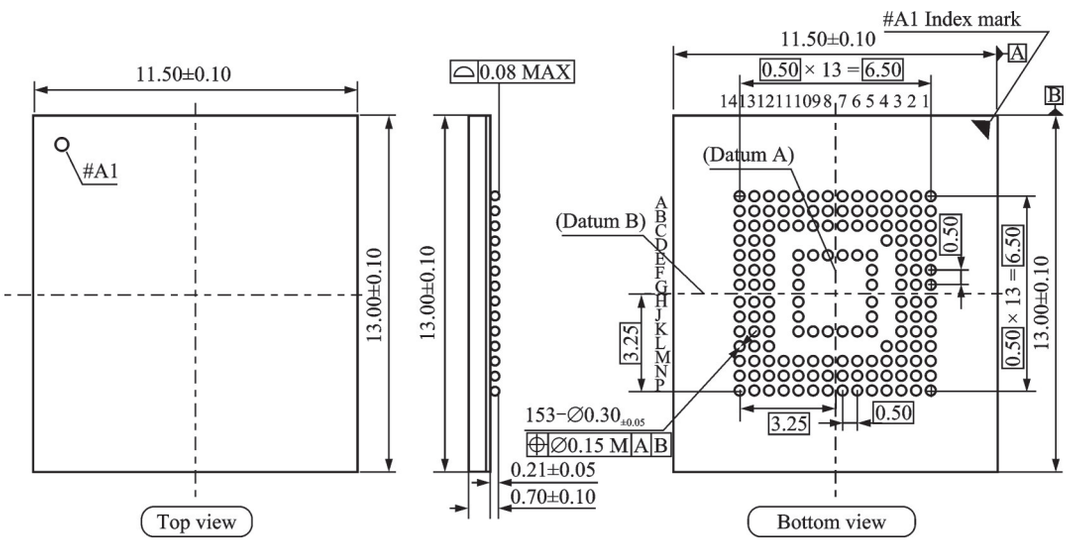

Fig.1 Size and structure of KLM8G1GETF-B041 chip package[22]

1.2 Thermal cycling test

In order to investigate the internal deformation of BGA package under thermal cycling loading, it is necessary to carry out thermal cycling test on the fabricated package sample. In this paper, the rapid temperature change test with specified conversion time in the GB/T2423.22—2002 standard for environmental testing of electrical and electronic products is referred. The thermal cycling loading curve is shown in Fig.2(a). The lowest temperature is set at −55 ℃, while the highest temperature is set at 125 ℃. Thus, a complete thermal cycle is "−55 ℃ — insulation — 125 ℃ — insulation — −55 ℃". The temperature holding time is 600 s, with a conversion time of 30 s, resulting in one cycle duration of 1 260 s. A total of 1 500 cycles are conducted in three rounds, with samples being taken out from the chamber for CT scanning after every 500 cycles. The thermal shock testing machine used for the thermal cycling test is shown in Fig.2(b). This machine, with its inner

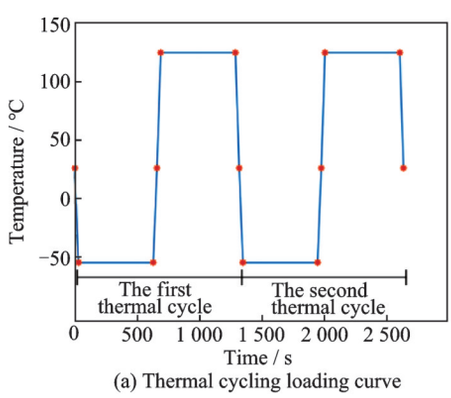

(a) Thermal cycling loading curve

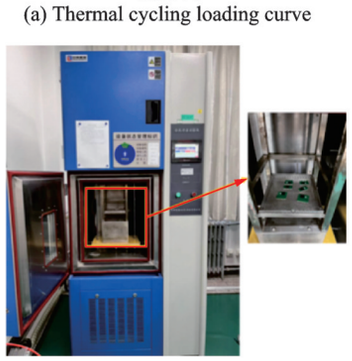

(b) Thermal shock testing machine

Fig.2 Thermal cycling loading curve and thermal shock testing machine

cavity mechanism, can automatically transfer the sample between the high and low temperature chambers.

1.3 CT imaging of BGA package

The nanoVoxel-4000 series micro-CT of Tianjin Sanying Precision Instrument Co., Ltd. was used for CT imaging, with the image resolution of 6.63 μm/pixel. A pre-test CT scan was performed before the thermal cycling test to acquire the reference volume image. The CT scan rotation angle was set to 360°, and a total of 1 080 projection images were acquired, with an exposure time of 0.8 s per image. Then the thermal cycling test was performed on the BGA package sample. The deformed volume images were collected after every 500 thermal cycles by removing the sample from the thermal chamber and conducting CT scans under the same settings as the pre-test scan. Consequently, in a single experiment, three loading sessions and four CT scans were performed: The reference volume image, the deformed volume images after 500 thermal cycles, 1 000 thermal cycles, and 1 500 thermal cycles.

2 Ex-situ Three-Dimensional Deformation Measurement Method

2.1 LW-RGDT DVC method

The volumetric images obtained by using X-ray CT in this paper have a large size of 1 400 voxel×2 500 voxel×500 voxel. Conventional DVC method usually reads the entire reference and deformed volume images during the calculation process, and even caches the interpolation coefficient of the entire deformed images for the subsequent subvoxel gray level interpolation. In this case, high-resolution volume images, comprising up to billions of voxels, need to be processed during DVC calculations, occupying a substantial amount of computer operating memory. These memory demands often exceed the hardware capabilities of personal computers. To address this, the LW-RGDT strategy is used in this paper. It divides the three-dimensional displacement tracking into reliability-guided propagation within layers and initial value propagation between layers. For the DVC calculation of each layer, only the reference layers centered on the current calculation layer in reference volume images and the deformation layers with adaptive sizes in deformation volume images are read into memory. This approach significantly reduces memory usage. The flowchart of LW-RGDT strategy is presented in Fig.3 and the detailed execution steps are as follows.

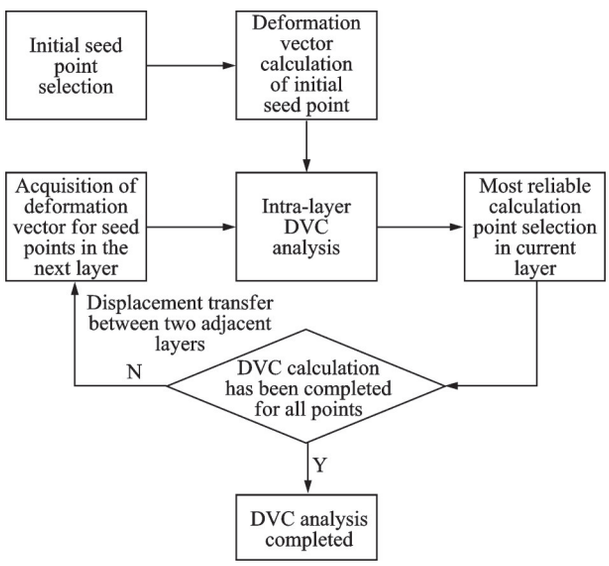

Fig.3 Flowchart of LW-RGDT strategy

Step 1 The estimation of initial value for seed point. After selecting the volume of interest (VOI) in the reference volumetric image, a seed point is specified at the top or bottom of the calculation area. For this seed point, an integer-displacement searching algorithm is employed to estimate the initial value. Based on this initial displacement, the three-dimensional inverse compositional Gauss-Newton (IC-GN) algorithm is then used to optimize the deformation vector, achieving a deformation vector with subvoxel accuracy.

Step 2 Intra-layer DVC analysis. After determining the deformation vector of the seed point, the intra-layer reliability-guided displacement propagation method is used to automatically transfer the deformation components of the calculated points to the adjacent points within the current calculation layer. Subsequently, the deformation vectors of these adja-

cent points can also be iteratively optimized using the three-dimensional IC-GN algorithm.

Step 3 Inter-layer DVC analysis. After finishing DVC analysis of the first layer, the point with the maximum zero-mean normalized cross-correlation (ZNCC) coefficient in the previous layer (the most reliable calculation point) is designated as the displacement transfer point. The deformation vector of this point is then transferred to the corresponding calculation point in the next layer using a simple first-order displacement shape function. Subsequently, the transferred point in the next layer is designated as the seed point for that layer, allowing the continuation of Step 2 in that layer. Finally, Steps 2 and 3 are repeated until all points within the calculation area have completed the DVC analysis.

Using the aforementioned LW-RGDT method, by establishing a layered data structure, the DVC calculation dynamically utilizes only the corresponding layered images in the reference and deformation volume images to track the deformation vectors of each calculation point. This approach minimizes the memory consumption of the DVC analysis, enabling the flexible handling of high-resolution volume images of the BGA package sample.

2.2 Rigid body displacement elimination method

To obtain the deformation field of package sample by DVC method, it is necessary to acquire the reference volume image and the deformed volume image of package sample before and after thermal cycling loading. Considering the limited internal space of the CT equipment and the lengthy duration of the thermal cycling test, ex-situ loading of the package sample is required. As shown in Fig.4, the displacement between the reference volume images and the deformed volume images of the sample consists of two parts, the rigid body displacement caused by ex-situ loading and structural deformation caused by thermal cycling load. Therefore, to accurately capture the deformation field of the package sample after thermal cycling loading, it is essential to develop an ex-situ DVC method to eliminate the influence of rigid body displacement.

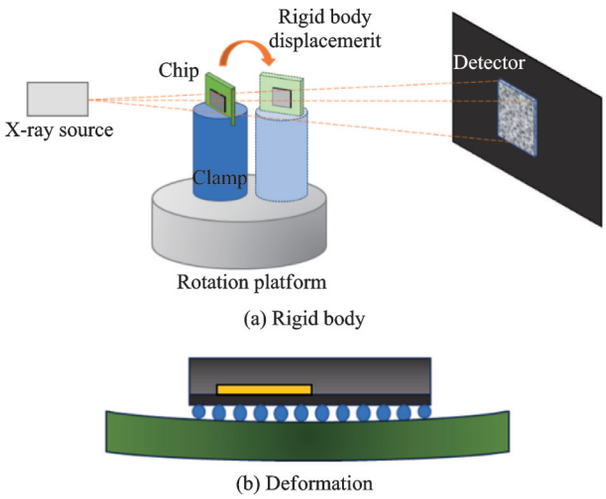

Fig.4 Rigid body displacement induced by ex-situ loading and deformation caused by thermal cycling loading

Point cloud data play an important role in computer vision and geometry processing tasks. However, point cloud data are often affected by rigid body displacement, complicating subsequent processing and analysis. Currently, the method for solving rigid body displacement based on SVD is widely used and yields favorable results.

In this paper, the package samples were repeatedly transferred between the thermal cycling test chamber and the X-ray CT scanning equipment. This procedure introduces significant rigid body displacement of the same sample at different test stages. This rigid body displacement information is coupled in the point cloud displacement field of the DVC calculations. Therefore, utilizing SVD method to eliminate rigid body displacements from the DVC data is highly appropriate

The SVD method is a matrix decomposition method that can decompose a matrix into the product of three matrices. For the point cloud data matrix computed by DVC, the SVD method can extract the information regarding rigid body transformations such as rotation, scaling and shift. Specifically, considering two point-clouds, one before deformation (reference point cloud matrix $\boldsymbol{P}_{3\times n}$) and one after deformation (deformation point cloud matrix $\boldsymbol{Q}_{3\times n}$)

$$\begin{cases} \boldsymbol{P}_{3\times n}=\left[\begin{bmatrix}x_1\\y_1\\z_1\end{bmatrix}_{P_1}\quad\begin{bmatrix}x_2\\y_2\\z_2\end{bmatrix}_{P_2}\quad\cdots\quad\begin{bmatrix}x_n\\y_n\\z_n\end{bmatrix}_{P_n}\right] \\ \boldsymbol{Q}_{3\times n}=\left[\begin{bmatrix}x_1\\y_1\\z_1\end{bmatrix}_{Q_1}\quad\begin{bmatrix}x_2\\y_2\\z_2\end{bmatrix}_{Q_2}\quad\cdots\quad\begin{bmatrix}x_n\\y_n\\z_n\end{bmatrix}_{Q_n}\right] \end{cases} \tag{1}$$

where (x_i, y_i, z_i) denotes the three-dimensional coordinates of corresponding points P_i and Q_i in the point cloud data, $i=1, 2, \cdots, n$.

The point clouds are decentralized by subtracting the centroid coordinates $\bar{\boldsymbol{P}}$ and $\bar{\boldsymbol{Q}}$ of each point cloud from the coordinates of each point within the point cloud, as shown in Eq.(2). The centroid coordinates are the mean coordinates of all points in the point cloud. The resulting coordinates, $\tilde{\boldsymbol{P}}$ and $\tilde{\boldsymbol{Q}}$, represent the decentralized coordinates of each point cloud.

$$\tilde{\boldsymbol{P}}=\boldsymbol{P}-\bar{\boldsymbol{P}},\ \tilde{\boldsymbol{Q}}=\boldsymbol{Q}-\bar{\boldsymbol{Q}} \tag{2}$$

According to Eq.(3), the covariance matrix $\boldsymbol{S}$ of two point-clouds is calculated. The matrix $\boldsymbol{W}$ represents the weight coefficient matrix for each point in the point cloud. In this context, all points weight equally in the point cloud, therefore $\boldsymbol{W}$ is the identity matrix $\boldsymbol{I}$. Performing SVD decomposition on $\boldsymbol{S}$ yields the diagonal matrix $\boldsymbol{\Sigma}$, which contains its singular values, as well as two orthogonal matrices $\boldsymbol{U}$ and $\boldsymbol{V}$ comprising the corresponding eigenvectors.

$$\tilde{\boldsymbol{P}}\boldsymbol{W}\tilde{\boldsymbol{Q}}^{\mathrm{T}}=\tilde{\boldsymbol{P}}\boldsymbol{I}\tilde{\boldsymbol{Q}}^{\mathrm{T}}=\boldsymbol{S},\ \boldsymbol{S}=\boldsymbol{U}\boldsymbol{\Sigma}\boldsymbol{V}^{\mathrm{T}} \tag{3}$$

The rigid body rotation matrix $\boldsymbol{R}$ and the rigid body translation vector $\boldsymbol{t}$ can be derived as

$$\boldsymbol{R}=\boldsymbol{V}\boldsymbol{U}^{\mathrm{T}},\ \boldsymbol{t}=\bar{\boldsymbol{Q}}-\boldsymbol{R}\bar{\boldsymbol{P}} \tag{4}$$

According to Eq.(5), The rigid body displacement field $\boldsymbol{D}_{\mathrm{rigid}}$ can be obtained by modifying the deformation point cloud with rotation matrix and rigid body translation matrix.

$$\boldsymbol{D}_{\mathrm{rigid}}=\boldsymbol{R}(\boldsymbol{P}+\boldsymbol{t})-\boldsymbol{P} \tag{5}$$

By subtracting the rigid body displacement obtained in Eq.(5) from the displacement results calculated by DVC, the influence of rigid body displacement in the DVC calculations can be eliminated.

2.3 Green's strain mapping

In the strain calculation from displacement fields, the Green's strain tensor, which is not affected by rigid body displacement and rigid body rotation, is chosen in this paper. Eq.(6) gives the Green's strain tensor components for the three-dimensional case.

$$\begin{cases} E_{12}=E_{21}=\dfrac{1}{2}(u_y+v_x+u_xu_y+v_xv_y+w_xw_y) \\ E_{13}=E_{31}=\dfrac{1}{2}(u_z+w_x+u_xu_z+v_xv_z+w_xw_z) \\ E_{23}=E_{32}=\dfrac{1}{2}(w_y+v_z+u_zu_y+v_zv_y+w_zw_y) \\ E_{11}=u_x+\dfrac{1}{2}\left[(u_x)^2+(v_x)^2+(w_x)^2\right] \\ E_{22}=v_y+\dfrac{1}{2}\left[(u_y)^2+(v_y)^2+(w_y)^2\right] \\ E_{33}=w_z+\dfrac{1}{2}\left[(u_z)^2+(v_z)^2+(w_z)^2\right] \end{cases} \tag{6}$$

where E represents the strain components, and u, v, w correspond to the displacement components in each spatial direction. The subscripts indicate the respective partial derivatives with respect to the spatial coordinates.

In the case of small deformations, the quadratic term is neglected and the Green's strain tensor degenerates into a small deformation tensor.

3 Results and Analysis

3.1 Preprocessing of X-ray CT image

The representative CT slice and 3D rendering of solder balls by X-ray CT are shown in Fig.5. The fine details within the package sample, including the solder balls and their internal voids, can be clearly observed. The noises and metal artifacts in the CT images may be due to the small-size solder balls and the sensitivity of the metal material present in the

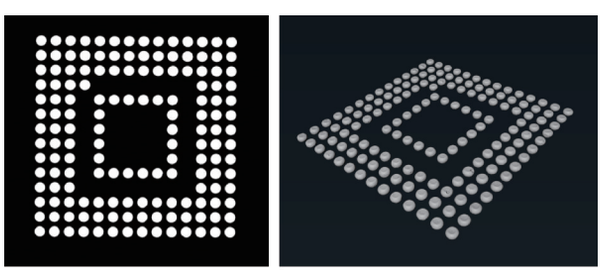

(a) A representative CT slice (b) 3D rendering of solder balls

Fig.5 A representative CT slice and 3D rendering of solder balls

package sample. In order to reduce the influence of metal artifacts and image noise in the reconstructed CT images on the DVC measurement accuracy, the images are filtered using a Gaussian filter to ensure that the image quality would not adversely affect the subsequent DVC calculation and analysis.

Before performing the DVC calculation based on the X-ray CT data, a coarse registration of the images was carried out according to the positions of the voids in the solder balls. Specifically, ImageJ was utilized to measure three prominent locations in the original images, which in this case correspond to three clearly visible void defects in the slice images. Subsequently, by manually adjusting the positions of these three distinct feature points before and after deformation, the volume images were preliminarily aligned, effectively eliminating large rigid body displacements. Fig.6 shows the comparisons of a representative slice between the reference volume image and the aligned deformed volume image. It can be observed that three marked void defects remain approximately parallel in the corresponding slices, and the boundary lines of the solder balls also exhibit a notable parallel alignment. The two sets of volume images were demonstrated to be roughly aligned based on visual inspection. It is worth noting that the coarse registration was employed to enhance the visibility of rigid body displacement patterns in the subsequent SVD calculation results, preventing these patterns from being obscured by large-scale rigid body translations. The effectiveness of the coarse registration step in eliminating large rigid body displacement does not significantly affect the accuracy of the subsequent SVD method.

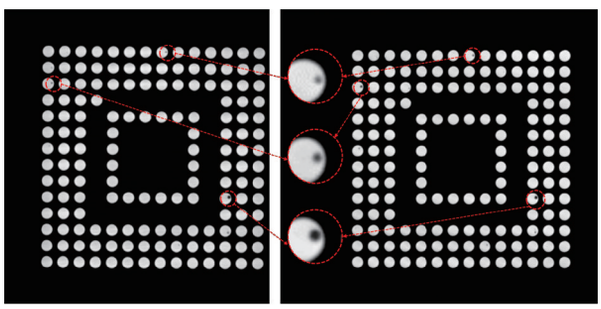

(a) Reference volume image (b) Aligned deformed volume image

Fig.6 A representative slice of the reference volume image and the aligned deformed volume image

3.2 Verification of rigid body displacement elimination method

To verify the effectiveness of extracting rigid body displacement by SVD method, a simulation test is carried out. A numerical simulation speckle with the size of 300 voxel×300 voxel×300 voxel is generated as the reference volume image, and then the rigid body displacement given by Eq.(7) is applied to generate the deformed image, where $\boldsymbol{R}$ is the rotation matrix and $\boldsymbol{t}$ the translation vector, as shown in Fig.7.

$$\boldsymbol{R}=\begin{bmatrix}\cos\frac{\pi}{6} & \sin\frac{\pi}{6} & 0\\ -\sin\frac{\pi}{6} & \cos\frac{\pi}{6} & 0\\ 0 & 0 & 1\end{bmatrix},\ \boldsymbol{t}=\begin{bmatrix}2\\3\\4\end{bmatrix} \tag{7}$$

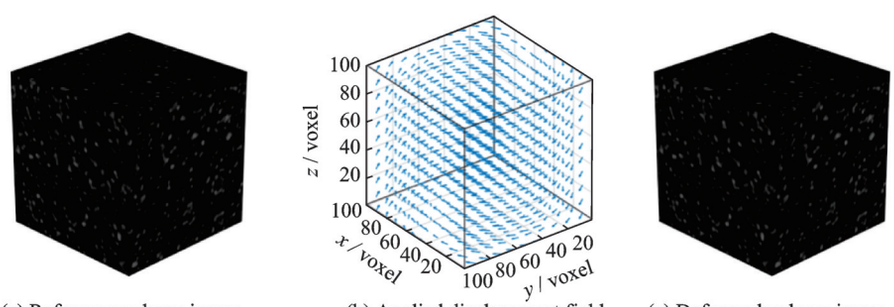

(a) Reference volume image (b) Applied displacement field (c) Deformed volume image

Fig.7 Simulation of rigid body displacement

The rigid body displacement field results from the SVD method are shown in Eq.(8), align with the displacement field applied by the simulation. This consistency indicates that the method used can extract rigid body displacement effective.

$$\boldsymbol{R}=\begin{bmatrix} 0.866\,0 & 0.500\,0 & 1.2\times10^{-17} \\ -0.500\,0 & 0.866\,0 & -2.2\times10^{-16} \\ -1.2\times10^{-17} & -3.2\times10^{-18} & 1.000\,0 \end{bmatrix},\ \boldsymbol{t}=\begin{bmatrix} 2.000\,0 \\ 3.000\,0 \\ 4.000\,0 \end{bmatrix} \tag{8}$$

3.3 Displacement measurement by ex-situ DVC method

The $\boldsymbol{U}$, $\boldsymbol{V}$ and $\boldsymbol{W}$ displacement fields of the calculation points after 500, 1 000 and 1 500 cycles of thermal cycling test are calculated using the conventional DVC method and the ex-situ DVC method, as shown in Figs.8(a) and (b), respectively. The size of subvolume is 81 voxel×81 voxel×81 voxel, and the step size is 20 voxels, resulting in a total of 15 126 uniformly distributed computational points. In Fig.8(b), the obtained true displacement results demonstrate that, following each thermal cycling, the BGA package consistently shows a tendency towards inward contraction. This behavior corresponds to the thermal cycling conditions depicted in Fig.2, particularly during the transition from low to

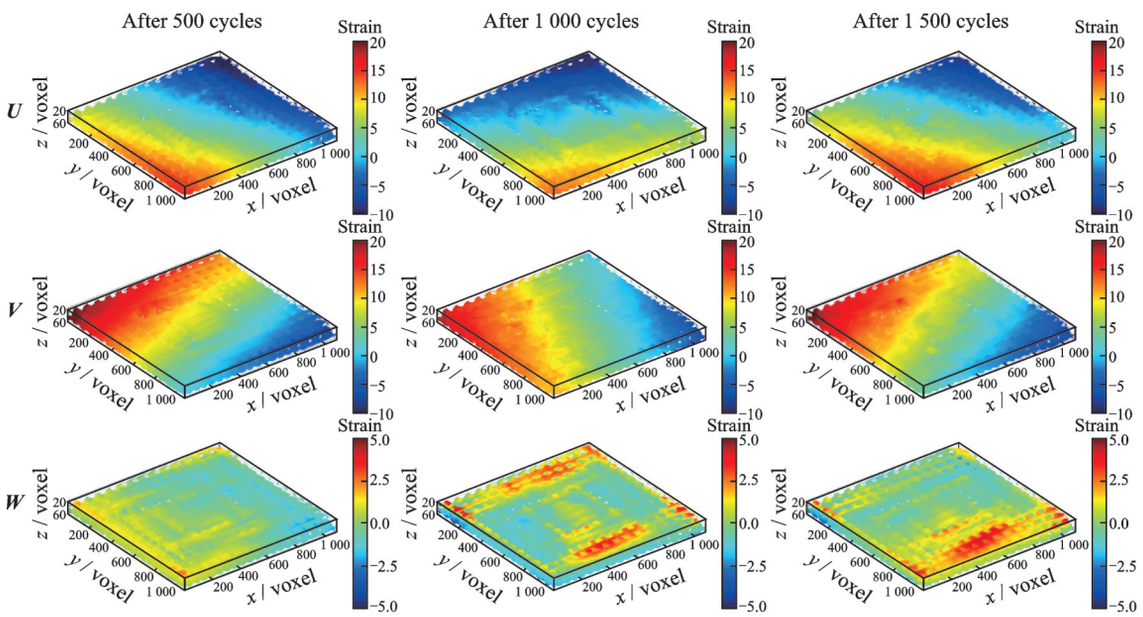

(a) Calculated by the conventional DVC method

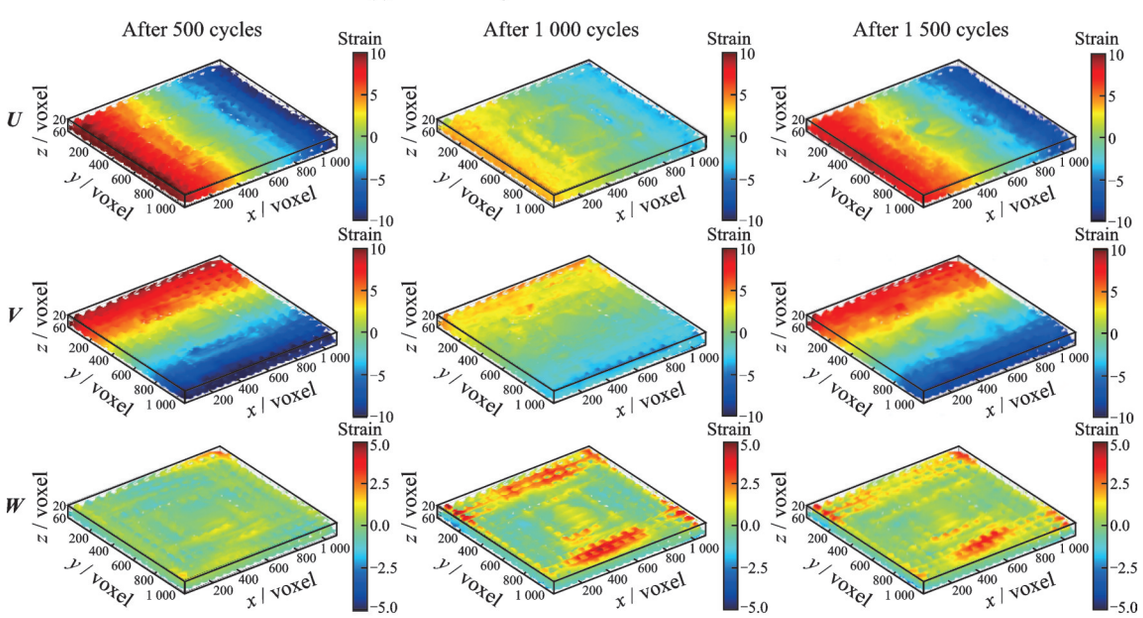

(b) Calculated by the ex-situ DVC method

Fig.8 Displacement field of the BGA package

ambient temperatures at the end of each thermal cycle. The displacement magnitude increases progressively from the center towards the edges of the BGA package, reaching its maximum at the periphery. This is especially evident in the z-direction displacement $\boldsymbol{W}$, where larger displacements are distinctly concentrated at the edges. This pattern is consisted with the deformation observed during in-situ thermal loading when the loading temperature is lower than the ambient temperature. In contrast, Fig.8(a) displays the displacement field without the removal of rigid body displacement, which is effectively the superposition of the displacement field from Fig.8(b) and the rigid body rotational displacement field in a counterclockwise direction around the center. This confirms that rigid body rotation has been effectively eliminated using the method proposed in this paper.

The obtained true displacement results demonstrate that, following each thermal cycling, the BGA package consistently shows a tendency towards inward contraction. This behavior corresponds to the thermal cycling conditions depicted in Fig.2, particularly during the transition from low to ambient temperatures at the end of each cycle. The displacement magnitude increases progressively from the center towards the edges of the BGA package, reaching its maximum at the periphery. This is especially evident in the z-direction displacement $\boldsymbol{W}$, where larger displacements are distinctly concentrated at the edges.

3.4 Verification of Green's strain

To verify the effectiveness of Green's strain in eliminating the effects of rigid body translation and rotation, the same simulation experiment in Section 3.2 is conducted. In the case of deformation involving only rigid body rotation and translation, the theoretical strain measurement results should be 0. Fig.9 shows the normal strain in x-direction of Cauchy strain and Green's strain extracted from the displacement field calculated by DVC. It can be observed that the Cauchy strain presents an average strain measurement error of 6.03×10^{-2}, while the

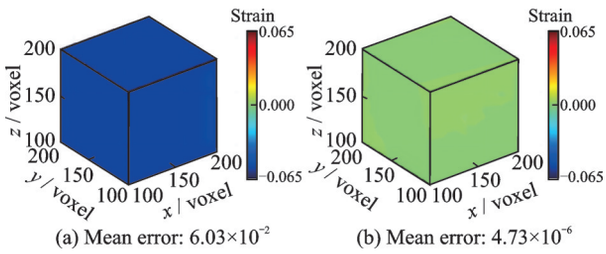

Fig.9 Cauchy strain and Green's strain extracted from the displacement field calculated by DVC

error of the Green's strain measurement result is only 4.73×10^{-6}. Compared with the Cauchy strain error, the Green's strain error is reduced by three orders of magnitude. Thus, it is proved that the Green's strain calculation method can effectively eliminate the effects of rigid body translation and rotation, and extract strain measurement results more accurately.

The strain field is derived by applying a suitable difference algorithm to the obtained displacement field, following the selection of an appropriate strain calculation method. It is important to acknowledge that noise is inherently present in the displacement field due to the influence of image noise. To address this, a point-by-point local least-squares fitting method is employed to calculate the strain field at each calculation point, utilizing a strain window size of $11\times11\times11$. This method effectively mitigates the impact of noise. The six resulting components (E_{11}, E_{22}, E_{33}, E_{12}, E_{13}, E_{23}) of Green's strain tensor for the BGA solder balls are presented in Fig.10.

3.5 Strain measurement by ex-situ DVC method

The strain component E_{33} exhibits a greater magnitude compared to the other strain components, as shown in Fig.10. Notably, the deformation of the solder balls is more significant at the corner positions, with E_{33} increasing in magnitude from the center towards the periphery. In contrast, the distribution of the other strain components remains relatively uniform across the BGA package.

The strain results indicate that the BGA package exhibits convex warping after every 500 cycles of thermal cycling test. This is due to the differing coefficients of thermal expansion of upper and lower

substrates of the BGA package, leading to different deformation under varying temperatures. This behavior is consistent with the convex warping phenomenon reported in the literature, as described in simulated thermal loading experiments of similar package structures[23].

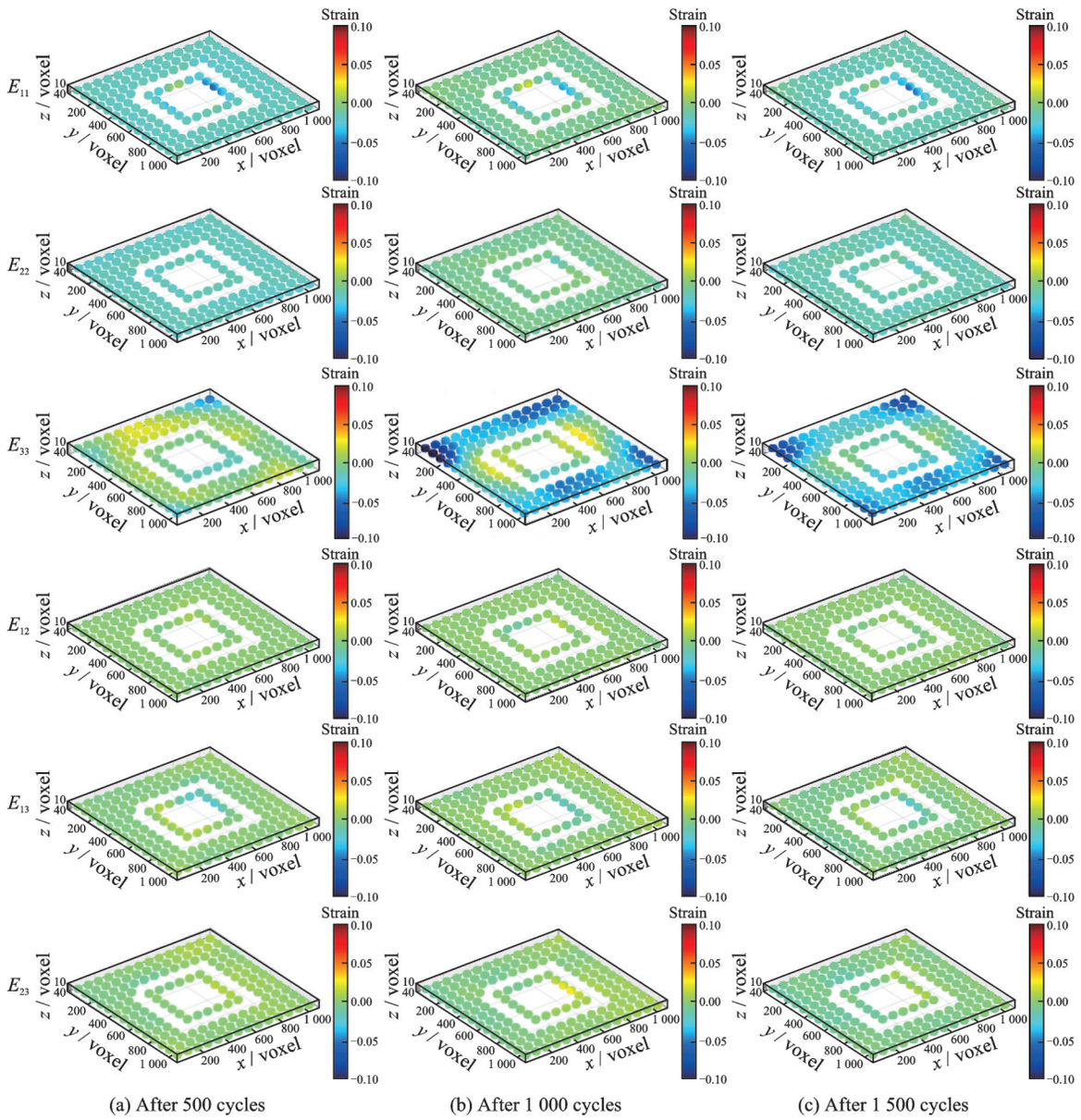

Fig.10 Six Green's strain components of BGA balls

4 Conclusions

The internal deformation of electronic package is difficult to be measured nondestructively due to the obstructions caused by the casing. Thus, the ex-situ measurement method for the internal deformation of electronic package based on X-ray CT imaging and DVC has been developed in this paper. The layer-wise reliability-guided displacement tracking strategy combined with SVD-based rigid body displacements elimination method has been employed. Using BGA packaging as a representative example, through the coarse alignment strategy and SVD method proposed in this study, we successfully obtained deformation field data for the package structure that is consistent with the deformation patterns observed in in-situ thermal loading experiments. This method effectively identified and eliminated the rigid body translations and rotations introduced

during ex-situ thermal cycling loading. The strain analysis results revealed a convex deformation characteristic, which aligns with the literature where simulation analyses based on differences in the thermal expansion coefficients of the upper and lower materials of the solder balls were conducted, thus validating the accuracy and reliability of the measurement techniques used in this study. This finding provides critical experimental evidence for accurately assessing the deformation behavior of package structures under thermal cycling conditions and offers an important reference and solution for precise measurement of chip package deformation under ex-situ loading conditions in future research.

Reference

[1] YANG Hao, MENG Qingkai, JIANG Bin. Controllability of spacecraft attitude and its application in reconfigurability analysis[J]. Transactions of Nanjing University of Aeronautics and Astronautics, 2019, 36(2): 189-196.

[2] GHAFFARIAN R. Book of Knowledge (BOK) for NASA electronic packaging roadmap: JPL-Publ-15-4[R]. [S.l.]: NASA, 2015.

[3] MEI Wang, YUAN Junshe, LIU Junyan, et al. Evaluation method of mechanical environment adaptability for rocket second-stage engine in the first-stage flight phase[J]. Journal of Rocket Propulsion, 2021, 47(4): 22-29.

[4] TANG Ye, LI Mingming, WANG Long, et al. Modeling and stability analysis of POGO vibration in liquid-propellant rockets with a two-propellant system[J]. Transactions of the Japan Society for Aeronautical and Space Sciences, 2017, 60(2): 77-84.

[5] JIN Y, BARATON X, YOON S, et al. Next generation eWLB (embedded wafer level BGA) packaging[C]//Proceedings of the 2010 12th Electronics Packaging Technology Conference.Singapore: [s.n.], 2010: 520-526.

[6] HOU Chuantao, WANG Long, CAO Liang, et al. Refined simulation method and failure study of BGA package structure based on image drive[J]. Microelectronics Journal, 2023,138: 105844.

[7] WANG Long, HOU Chuantao, ZHENG Junxing, et al. Automated coplanarity inspection of BGA solder balls by structured light[J]. Microelectronics Journal, 2023, 138: 105802.

[8] DEPIVER J A, MALLIK S, AMALU E H. Thermal fatigue life of ball grid array (BGA) solder joints made from different alloy compositions[J]. Engineering Failure Analysis, 2021, 125: 105447.

[9] DEPIVER J A, MALLIK S, AMALU E H. Creep response of various solders used in soldering ball grid array (BGA) on printed circuit board (PCB)[C]// Proceedings of World Congress on Engineering and Computer Science. Sans Francisco, California, USA: [s.n.], 2019.

[10] ZHANG J, LI M, XIONG C Y, et al. Thermal deformation analysis of BGA package by digital image correlation technique[J]. Microelectronics International, 2005, 22(1): 34-42.

[11] BAY B K, SMITH T S, FYHRIE D P, et al. Digital volume correlation: Three-dimensional strain mapping using X-ray tomography[J]. Experimental Mechanics, 1999, 39: 217-226.

[12] WANG Long, FENG Guolin, LI Zhiqiang, et al. Applications of X-ray computed tomography to study the mechanical behaviors of materials[J]. Structure & Enviroment Engineering, 2017, 44(6): 43-56.

[13] GAO Xiangxi, YANG Pinghua, QIAO Haiyan, et al. Defect characteristics within SLM-fabricated GH3536 superalloy dependence on μCT characterization[J]. Journal of Materials Engineering, 2022, 50(10): 63-72.

[14] WANG Long, JIA Zhouxia, LI Zhiqiang, et al. Mechanical measurement of electronic components by using X-ray CT and DVC method[J]. Structure & Enviroment Engineering, 2019, 46(1): 49-56.

[15] WANG B, PAN B, LUBINEAU G. Morphological evolution and internal strain mapping of pomelo peel using X-ray computed tomography and digital volume correlation[J]. Materials and Design, 2018, 137: 305-315.

[16] WANG Long, YUAN Kai, LUAN Xingang, et al. 3D Characterizations of pores and damages in C/SiC composites by using X-ray computed tomography[J]. Applied Composite Materials, 2019, 26(2): 493-505.

[17] XIANG Z, BING P. Particle-volume tracking-assisted discrete digital volume correlation for kinematics analysis of particles[J]. Granular Matter, 2023. DOI: 10.1007/s10035-022-01292-w.

[18] WANG Long, ZHANG Wei, LI Haibo, et al. 3D in-situ characterizations of damage evolution in C/SiC composite under monotonic tensile loading by using X-ray computed tomography[J]. Applied Composite Materials, 2020, 27(3): 119-130.

[19] PAN B, WANG B, WU D, et al. An efficient and ac-

curate 3D displacements tracking strategy for digital volume correlation[J]. Optics and Lasers in Engineering, 2014, 58: 126-135.

[20] WAN K, YANG P. Expanded digital volume correlation for ex situ applications[J]. Measurement Science and Technology, 2015, 26(9): 095605.

[21] PAN B, WANG B. A flexible and accurate digital volume correlation method applicable to high-resolution volumetric images[J]. Measurement Science and Technology, 2017, 28(10): 105007.

[22] Samsung Electronics. Samsung eMMC product family KLM8G1GETF-B041 datasheet[EB/OL]. [2024-08-20]. https://www.samsung.com.cn.

[23] HIROHATA K, HISANO K, MUKAI M, et al. Coupled thermal-stress analysis for FC-BGA packaging reliability design[J]. IEEE Transactions on Components and Packaging Technologies, 2010, 33(2): 347-358.

Authors Dr. **WANG Long** received the B.S. and M.S. degrees in mechanics from School of Astronautics, Harbin Institute of Technology, China, in 2009 and 2011, respectively, and the Ph.D. degree in mechanics from the Laboratoire de Mécanique de Lille (LML), CNRS, UMR 8107, Ecole Centrale de Lille, France, in 2015. He is currently a senior engineer in Science and Technology on Reliability and Environmental Engineering Laboratory, Beijing Institute of Structure and Environment Engineering, Beijing, China. His research interests include non-destructive testing and evaluation of equipment, and experimental solid mechanics.

Mr. **GAO Zizhan** has been pursuing his Ph.D. degree at School of Aeronautic Science and Engineering of Beihang University. His main research focuses on digital volume correlation and rapid CT image reconstruction using deep learning.

Author contributions Dr. **WANG Long** designed the study, conducted the analysis, and wrote the original manuscript. Mr. **GAO Zizhan** helped to review and edit the manuscript, and contributed to discussion and background of the study. Mr. **ZHANG Xuanhao** contributed to the proofreading of the manuscript. Dr. **HOU Chuantao**, Mr. **LIU Qiaoyu**, and Dr. **XING Ruisi** contributed to discussion and background of the study. All authors commented on the manuscript draft and approved the submission.

Competing interests The authors declare no competing interests.

(Production Editor: ZHANG Huangqun)

球栅阵列电子封装结构内部变形的非原位数字体图像相关方法研究

王 龙[1], 高子展[2], 张轩豪[2], 刘乔雨[1], 侯传涛[1], 邢睿思[1]

(1.北京强度环境研究所可靠性与环境工程技术重点实验室,北京 100076,中国; 2.北京航空航天大学航空科学与工程学院强度与结构完整性全国重点实验室,北京 100191,中国)

摘要:在航天器电子设备中,球栅阵列(Ball grid array, BGA)封装内焊球的变形会对系统可靠性造成重大影响。因此,精确测量焊球的力学行为对确保航天器的安全性和可靠性至关重要。尽管有限元仿真已被广泛应用于研究焊球变形,但在热循环条件下,其实验数据验证仍有缺失。这一现象主要归因于准确测量焊球变形以及消除离位热循环加载中刚体位移的挑战。为克服这些难题,本文提出了一种基于X射线计算机断层扫描(Computed tomography, CT)和数字体图像相关(Digital volume correlation, DVC)的离位三维变形测量方法。该方法结合逐层可靠性导向位移跟踪(Layer-wise reliability-guided displacement tracking, LW-RGDT)DVC与奇异值分解(Singular value decomposition, SVD)方法,能够不受刚体位移影响,精确评估BGA封装结构中焊球的力学行为。实验结果表明,随着热循环次数的增加,BGA结构出现了逐渐显著的凸状变形,尤其是边缘焊球的变形更为明显。这一方法为离位条件下评估电子封装内部变形提供了可靠而有效的工具,对其设计优化与寿命预测具有重要意义。

关键词:球栅阵列封装;数字体图像相关;离位;刚体位移;热循环测试